Supporting Information

# 2D AuPd alloy nanosheets: one-step synthesis as imaging-guided photonic nano-antibiotics

Songliang He,[a,#] Guoshuai Zhu,[a,#] Zhencheng Sun,[a] Jidong Wang,[b,c] Ping Hui,[a] Penghe Zhao,[a] Wenwen Chen*[,a,c] and Xingyu Jiang[d]

[a] Guangdong Key Laboratory for Biomedical Measurements and Ultrasound Imaging, School of Biomedical Engineering, Shenzhen University Health Science Center, Shenzhen 518055, China

[b] Central Laboratory, Huazhong University of Science and Technology union Shenzhen Hospital (Nanshan Hospital), Shenzhen Nanshan People's Hospital and the 6th Affiliated Hospital of Shenzhen University Health Science Center, Shenzhen 518052, China

[c] John A. Paulson School of Engineering and Applied Sciences, Harvard University, Cambridge, MA 02138, USA

[d] Department of Biomedical Engineering, Southern University of Science and Technology, Shenzhen 518055, China

* Corresponding author, E-mail: chenww@szu.edu.cn

[#] These authors equally contributed to the work

## Table of Contents

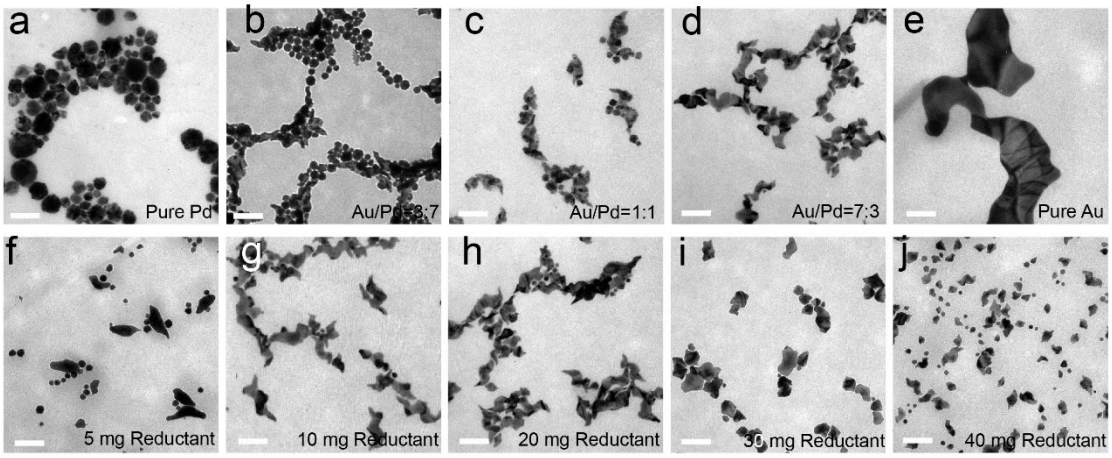


**Figure S1.** TEM images of Au, Pd, or AuPd nanosheets synthesized in different conditions (reductant is sodium ascorbate, scale bars are 100 nm). a) Pure Pd. b) 3 : 7 mole ratio for Au and Pd. c) 1 : 1 mole ratio for Au and Pd. d) 7 : 3 mole ratio for Au and Pd. e) Pure Pd. f-j) AuPd synthesized using different reductant consumption (5, 10, 20, 30, and 40 mg) with 7 : 3 mole ratio for Au and Pd.

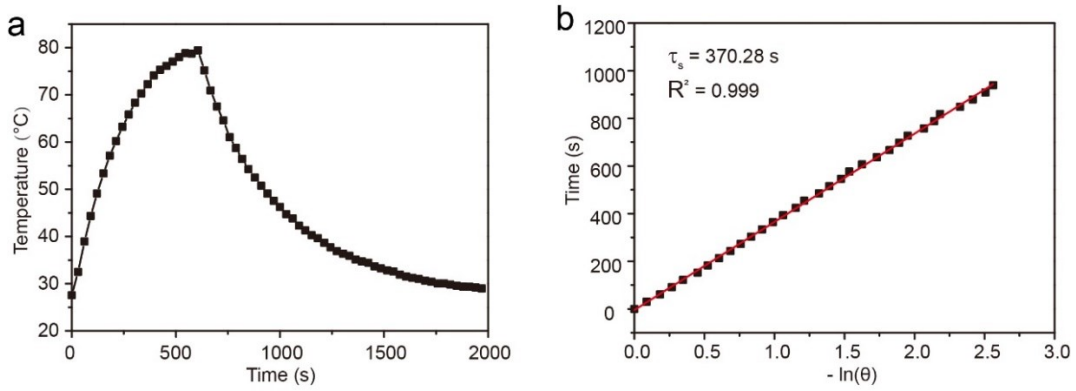


**Figure S2.** a) Monitored temperature profile of AuPd nanosheets (50 μg/mL) within 30 min irradiated by 808 nm laser (1 W/cm$^2$). b) Linear dependent curve between cooling time and temperature related variable (-ln ɵ) for calculating time constant $\tau_s$ of spontaneous cooling system.

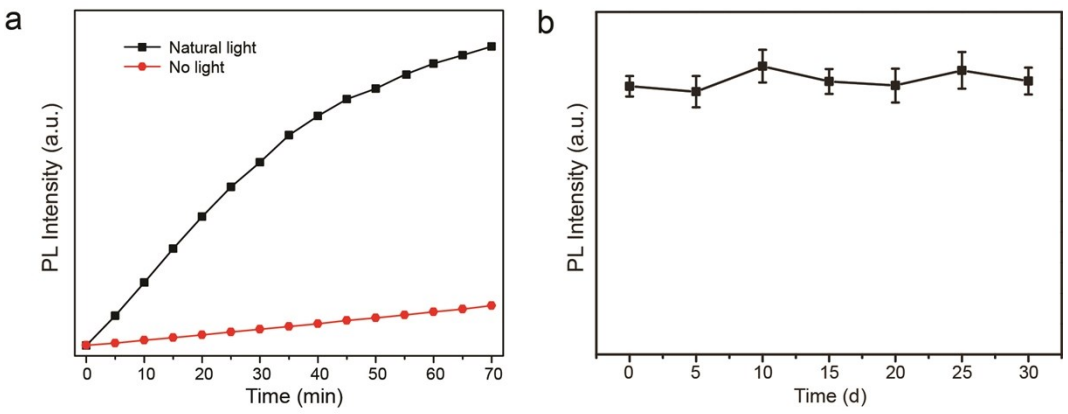


**Figure S3.** a) Fluorescent intensity of DCFH mixed with AuPd nanosheets at 525 nm under natural light and dark conditions respectively with time. b) Fluorescent intensity of DCFH mixed with AuPd nanosheets at 525 nm recorded after 808 nm laser irradiation (1 W/cm$^2$) for 1 min, which was measured every 5 days during a month.

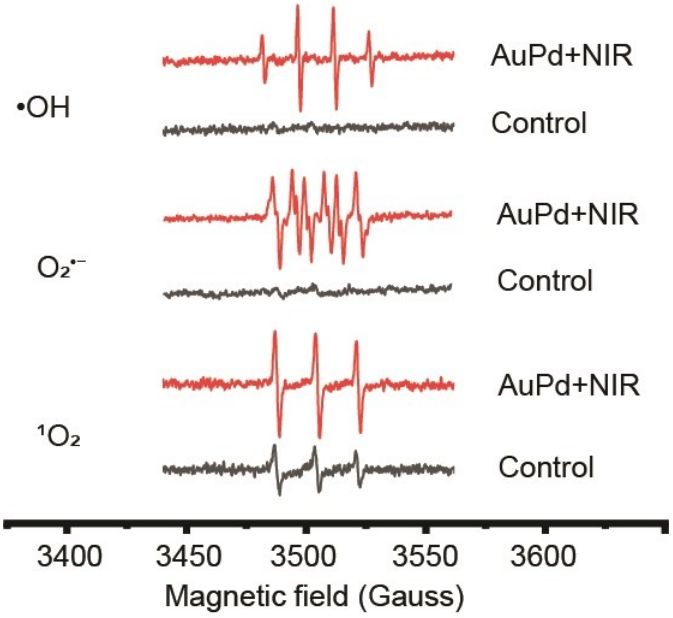


**Figure S4.** Investigation of reactive oxygen species production of AuPd nanosheets by electron paramagnetic resonance (EPR). Under 808 nm laser irradiation for 5 min (1 W cm$^{-2}$), $^1O_2$, $O_2^{\bullet-}$, and •OH generation of AuPd nanosheets were evaluated by EPR. Control: solvent (water) + trapping agent (TEMP or DMPO), under 808 nm laser irradiation for 5 min (1 W/cm$^2$). TEMP was used as $^1O_2$ trapping agent and DMPO was used as $O_2^{\bullet-}$, and •OH trapping agent.

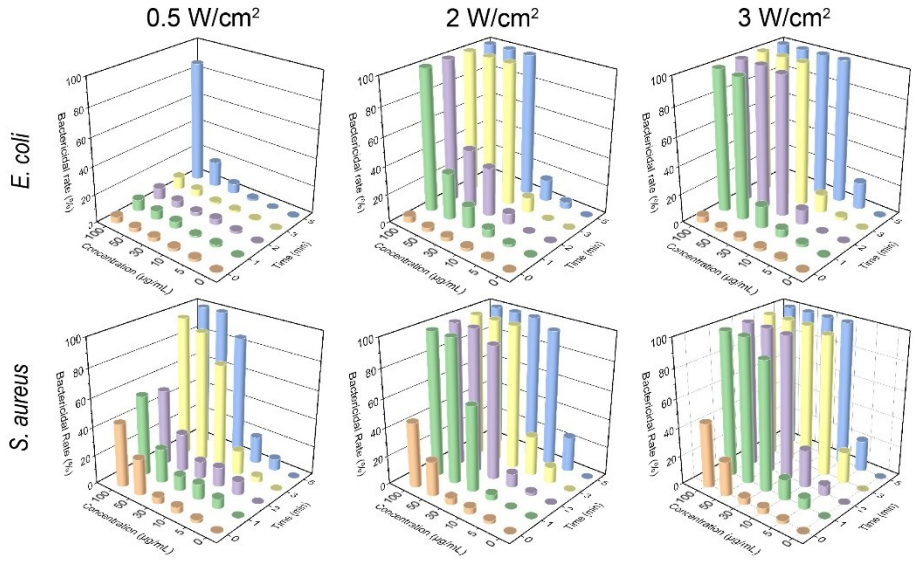


**Figure S5.** Antibacterial activity for *E. coli* and *S. aureus* under various power densities (0.5, 2, and 3 W/cm$^2$), irradiated time (0, 1, 2, 3, and 5 min), and concentrations (0, 5, 10, 30, 50, and 100 μg/mL) of AuPd nanosheets.

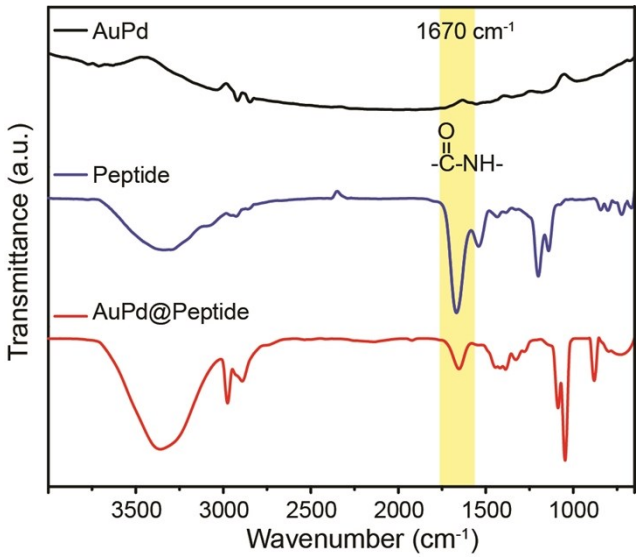


**Figure S6.** a) UV-Vis spectra of AuPd, peptide, and AuPd@Peptide. b) Infrared spectra of AuPd, peptide, and AuPd@Peptide.

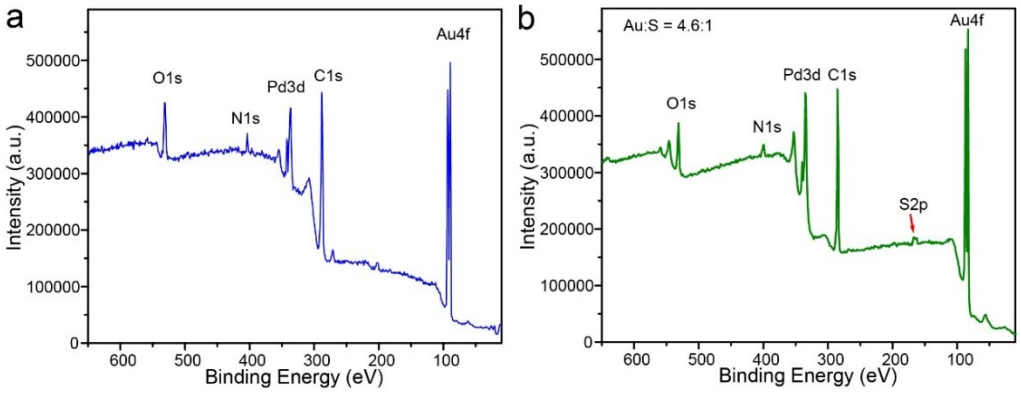


**Figure S7.** XPS analysis of AuPd nanosheets before and after peptides modification.

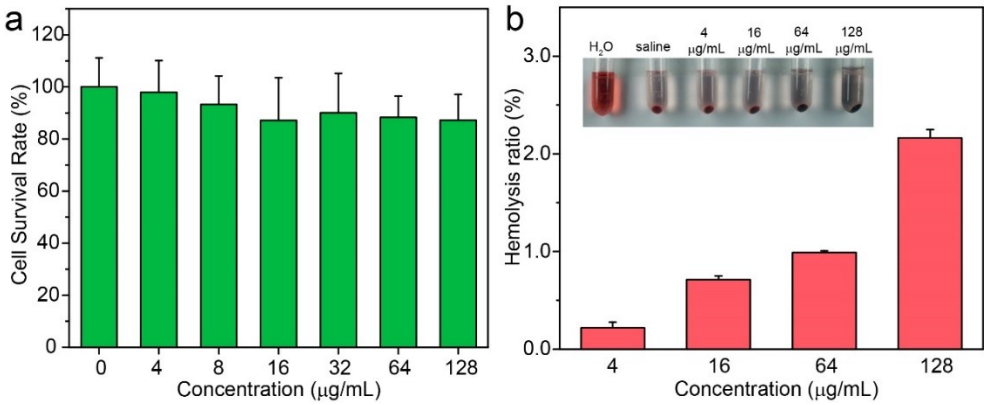


**Figure S8.** a) Cytotoxicity assay of AuPd@Peptide. b) Hemolysis assay of AuPd@Peptide, insert was photograph of different treated samples.

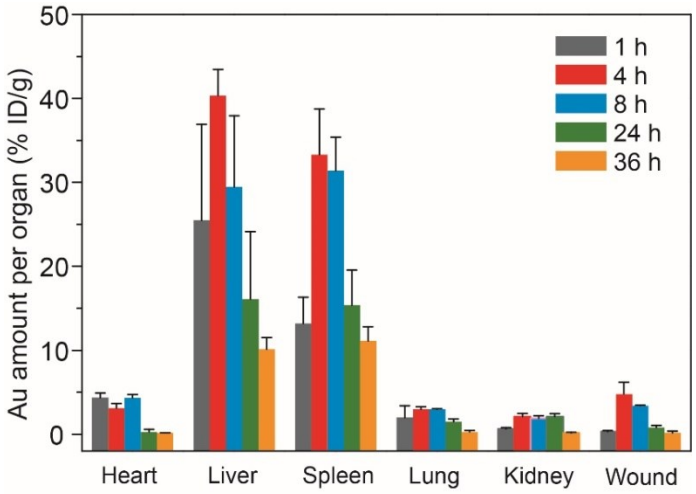


**Figure S9.** Quantitative analysis of Au amount per organ in infected mice with time.

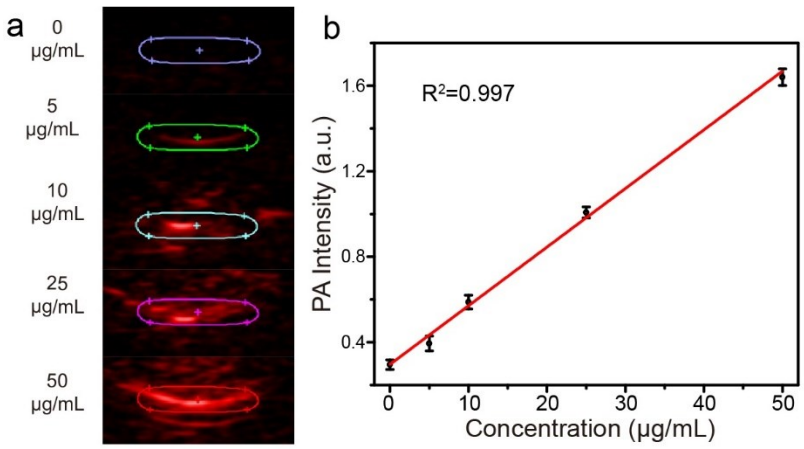


**Figure S10.** Characterization of photoacoustic properties of AuPd nanosheets. a) In vitro PAI of AuPd nanosheets with different concentrations. b) Linear relationship between the concentrations and the PA signals in a).

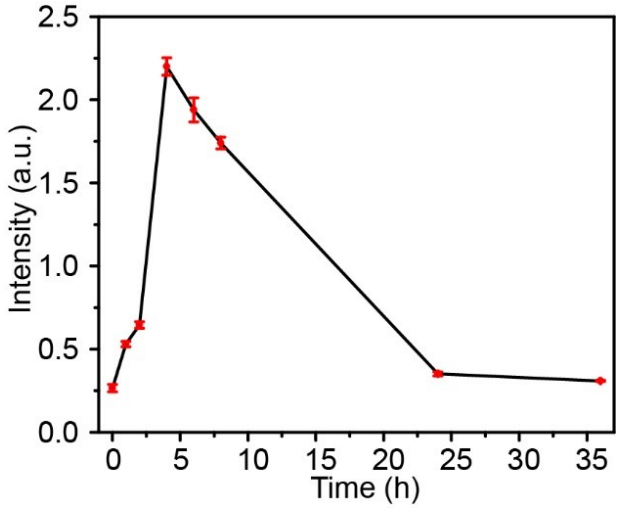


**Figure S11.** Quantitative analysis of PA signals in infected regions of mice with time.

**Table S1.** Morphology and photothermal conversion efficiency of some reported photothermal nanomaterials.

| Materials | Morphology | Photothermal efficiency | Reference |
|---|---|---|---|
| AuPd | nanoplates | 76.6% | This work |
| Au | nanorods | 21% | [1] |
| Au-PEI@pD | nanostars | 49.9% | [2] |
| Pd | nanoparticles | 93.4% | [3] |
| Pd | nanosheets | 52% | [4] |
| Pd@Au | nanoplates | 28.6% | [5] |
| GNS@PDA | nanostars | 36.5% | [6] |
| SCN-$Zn^{2+}$@GO | nanosheets | 21.8% | [7] |
| PEG-$MoS_2$ | nanoflowers | 43.72% | [8] |
| $MoS_2$-CS | nanosheets | 24.37% | [9] |
| BiOI@$Bi_2S_3$ | nanoparticles | 28.5% | [10] |
| UiO-66@PAN hybrids | nanoparticles | 21.6% | [11] |
| PDA-Ce6 | nanoparticles | 40% | [12] |
| Peptide porphyrin conjugate | nanodots | 54.2% | [13] |
| $Ti_3C_2$ | nanosheets | 30.6% | [14] |
| $MoO_{3-x}$ | hollow nanospheres | 22.64% | [15] |
| $MoSe_2$ | nanodots | 46.5% | [16] |

**Table S2.** Minimum inhibitory concentration of AuPd nanosheets with different power and time conditions.

| | Concentration of AuPd nanosheets (μg/mL) | | | | | | | |
|---|---|---|---|---|---|---|---|---|
| Bacteria species | *E. coli* | | | | *S. aureus* | | | |
| Irradiation power | Time (min) | | | | Time (min) | | | |
| ($W/cm^2$) | 1 | 2 | 3 | 5 | 1 | 2 | 3 | 5 |
| 0.5 | >100 | >100 | >100 | >100 | 80 | 80 | 40 | 10 |
| 1 | >100 | 80 | 50 | 40 | 40 | 20 | 10 | 10 |
| 2 | 50 | 50 | 30 | 25 | 10 | 10 | 10 | 10 |
| 3 | 50 | 30 | 20 | 10 | 10 | 10 | 10 | 10 |

**Table S3.** Minimal bactericidal concentration of AuPd nanosheets with different power and time conditions.

| | Concentration of AuPd nanosheets (μg/mL) | | | | | | | |
|---|---|---|---|---|---|---|---|---|
| Bacteria species | *E. coli* | | | | *S. aureus* | | | |
| Irradiation power | Time (min) | | | | Time (min) | | | |
| ($W/cm^2$) | 1 | 2 | 3 | 5 | 1 | 2 | 3 | 5 |
| 0.5 | >100 | >100 | >100 | >100 | >100 | >100 | >100 | 40 |
| 1 | >100 | >100 | 55 | 50 | >100 | 60 | 40 | 15 |
| 2 | 80 | 75 | 30 | 25 | 45 | 35 | 30 | 15 |
| 3 | 55 | 35 | 25 | 10 | 40 | 30 | 15 | 10 |

**Table S4.** Effects of AuPd@Peptide on biomedical health indicators in blood of mice injected 7 days later.

| Groups | Control (N=5) | AuPd@Peptide (N=5) |
|---|---|---|
| WBC ($10^9$/L) | 7.20 ±1.38 | 7.00 ±1.45 |
| RBC ($10^{12}$/L) | 10.02 ±0.12 | 10.26 ±0.18 |
| PLT ($10^9$/L) | 669.75 ±110.40 | 674.00 ±100.86 |
| MCV (fL) | 45.23 ±1.50 | 46.67 ±2.83 |
| MCHC (g/L) | 411.50 ±47.75 | 409.75 ±18.82 |
| ALP (U/L) | 130.3 ± 10.5 | 125.0 ± 17.8 |
| ALT (U/L) | 43.3 ± 5.7 | 43.0 ± 9.6 |
| AST (U/L) | 158.0 ± 27.0 | 156.0 ± 18.0 |
| Cre (μM) | 37.0 ± 5.2 | 38.7 ± 8.1 |
| UREA (mM) | 10.5 ± 1.0 | 9.6 ± 1.2 |

Abbreviation in table: White Blood Cell (WBC), Red Blood Cell (RBD), Platelet (PLT), Mean Corpuscular Volume (MCV), Mean Corpuscular Hemoglobin Concentration (MCHC), Alkaline Phosphatase (ALP), Alanine Aminotransferase (ALT), Aspartate Aminotransferase (AST), creatinine (Cre).

**References**


[1] J. Zeng, D. Goldfeld, Y. Xia, A plasmon-assisted optofluidic (PAOF) system for measuring the photothermal conversion efficiencies of gold nanostructures and controlling an electrical switch, Angew Chem Int Ed Engl 52(15) (2013) 4169-4173.

[2] D. Li, Y. Zhang, S. Wen, Y. Song, Y. Tang, X. Zhu, M. Shen, S. Mignani, J.-P. Majoral, Q. Zhao, X. Shi, Construction of polydopamine-coated gold nanostars for CT imaging and enhanced photothermal therapy of tumors: an innovative theranostic strategy, Journal of Materials Chemistry B 4(23) (2016) 4216-4226.

[3] J.W. Xiao, S.X. Fan, F. Wang, L.D. Sun, X.Y. Zheng, C.H. Yan, Porous Pd nanoparticles with high photothermal conversion efficiency for efficient ablation of cancer cells, Nanoscale 6(8) (2014) 4345-4351.

[4] S. Tang, M. Chen, N. Zheng, Sub-10-nm Pd nanosheets with renal clearance for efficient near-infrared photothermal cancer therapy, Small 10(15) (2014) 3139-3144.

[5] M. Chen, S. Tang, Z. Guo, X. Wang, S. Mo, X. Huang, G. Liu, N. Zheng, Core-shell Pd@Au nanoplates as theranostic agents for in-vivo photoacoustic imaging, CT imaging, and photothermal therapy, Adv Mater 26(48) (2014) 8210-8216.

[6] X. Han, Y. Xu, Y. Li, X. Zhao, Y. Zhang, H. Min, Y. Qi, G.J. Anderson, L. You, Y. Zhao, G. Nie, An Extendable Star-Like Nanoplatform for Functional and Anatomical Imaging-Guided Photothermal Oncotherapy, ACS Nano 13(4) (2019) 4379-4391.

[7] Y. Li, X. Liu, L. Tan, Z. Cui, X. Yang, Y. Zheng, K.W.K. Yeung, P.K. Chu, S. Wu, Rapid Sterilization and Accelerated Wound Healing Using $Zn^{2+}$ and Graphene Oxide Modified g-$C_3N_4$ under Dual Light Irradiation, Advanced Functional Materials 28(30) (2018) 1800299.

[8] W. Yin, J. Yu, F. Lv, L. Yan, L.R. Zheng, Z. Gu, Y. Zhao, Functionalized Nano-$MoS_2$ with Peroxidase Catalytic and Near-Infrared Photothermal Activities for Safe and Synergetic Wound Antibacterial Applications, ACS Nano 10(12) (2016) 11000-11011.

[9] W.Y. Yin, L. Yan, J. Yu, G. Tian, L.J. Zhou, X.P. Zheng, X. Zhang, Y. Yong, J. Li, Z.J. Gu, Y.L. Zhao, High-Throughput Synthesis of Single-Layer $MoS_2$ Nanosheets as a Near-Infrared Photothermal-Triggered Drug Delivery for Effective Cancer Therapy, ACS Nano 8(7) (2014) 6922-6933.

[10] Z. Guo, S. Zhu, Y. Yong, X. Zhang, X. Dong, J. Du, J. Xie, Q. Wang, Z. Gu, Y. Zhao, Synthesis of BSA-Coated BiOI@$Bi_2S_3$ Semiconductor Heterojunction Nanoparticles and Their Applications for Radio/Photodynamic/Photothermal Synergistic Therapy of Tumor, Adv Mater 29(44) (2017).

[11] W. Wang, L. Wang, Y. Li, S. Liu, Z. Xie, X. Jing, Nanoscale Polymer Metal-Organic Framework Hybrids for Effective Photothermal Therapy of Colon Cancers, Adv Mater 28(42) (2016) 9320-9325.

[12] D. Zhang, M. Wu, Y. Zeng, L. Wu, Q. Wang, X. Han, X. Liu, J. Liu, Chlorin e6 Conjugated Poly(dopamine) Nanospheres as PDT/PTT Dual-Modal Therapeutic

Agents for Enhanced Cancer Therapy, ACS Appl Mater Interfaces 7(15) (2015) 8176-8187.
[13] Q. Zou, M. Abbas, L. Zhao, S. Li, G. Shen, X. Yan, Biological Photothermal Nanodots Based on Self-Assembly of Peptide-Porphyrin Conjugates for Antitumor Therapy, J Am Chem Soc 139(5) (2017) 1921-1927.
[14] H. Lin, X. Wang, L. Yu, Y. Chen, J. Shi, Two-Dimensional Ultrathin MXene Ceramic Nanosheets for Photothermal Conversion, Nano Lett 17(1) (2017) 384-391.
[15] T. Bao, W. Yin, X. Zheng, X. Zhang, J. Yu, X. Dong, Y. Yong, F. Gao, L. Yan, Z. Gu, Y. Zhao, One-pot synthesis of PEGylated plasmonic $MoO_{(3-x)}$ hollow nanospheres for photoacoustic imaging guided chemo-photothermal combinational therapy of cancer, Biomaterials 76 (2016) 11-24.
[16] L. Yuwen, J. Zhou, Y. Zhang, Q. Zhang, J. Shan, Z. Luo, L. Weng, Z. Teng, L. Wang, Aqueous phase preparation of ultrasmall $MoSe_2$ nanodots for efficient photothermal therapy of cancer cells, Nanoscale 8(5) (2016) 2720-2726.